Nucl. Fusion **52** (2012) 043001 (10pp) doi:10.1088/0029-5515/52/4/043001

# Observation of global Alfvén eigenmode avalanche events on the National Spherical Torus Experiment

**E.D. Fredrickson[1], N.N. Gorelenkov[1], E. Belova[1], N.A. Crocker[2], S. Kubota[2], G.J. Kramer[1], B. LeBlanc[1], R.E. Bell[1], M. Podesta[1], H. Yuh[3] and F. Levinton[3]**

[1] Princeton Plasma Physics Laboratory, Princeton, NJ 08543, USA
[2] University of California, Los Angeles, CA 90095, USA
[3] Nova Photonics, Princeton, NJ 08543, USA

E-mail: efredrickson@pppl.gov

Received 2 November 2011, accepted for publication 21 December 2011
Published 19 March 2012
Online at stacks.iop.org/NF/52/043001

**Abstract**
Instabilities excited by the fast-ion population on NSTX (Ono *et al* 2000 *Nucl. Fusion* **40** 557) extend from low-frequency energetic particle modes (EPMs) at tens of kHz through toroidal Alfvén eigenmodes (TAEs) in the range 50–150 kHz to global and compressional Alfvén eigenmodes (GAE and CAE) in the frequency range 0.3–2.5 MHz, or roughly $0.1\omega_{ci}$ to $0.7\omega_{ci}$. The GAE instabilities exhibit complex non-linear behaviour, including onset of strong growth above an amplitude threshold. This is conjectured to occur when resonance regions in phase space start to overlap, resulting in enhanced rapid growth and redistribution of energetic particles, a process referred to as an 'avalanche' (Berk *et al* 1995 *Nucl. Fusion* **35** 1661). The GAE are suppressed following the avalanche, suggesting depletion of the fast-ion population resonantly driving the modes, and in some instances the GAE bursts appear to trigger lower frequency TAE avalanches or EPMs, suggesting some significant redistribution of fast ions in phase space has occurred. These are the first reported observations of avalanching behaviour for an instability driven through the Doppler-shifted cyclotron resonance. This paper also provides internal measurements of GAE structure showing that the mode amplitude peaks towards the plasma core.

(Some figures may appear in colour only in the online journal)

## 1. Introduction

The National Spherical Torus Experiment (NSTX) [1] is a low aspect ratio ($A = R/a \approx 1.5$) tokamak with maximum toroidal field of up to 5.5 kG, plasma current of up to ≈1.2 MA and neutral beam injection (NBI) heating of up to ≈6 MW with 60 kV to 90 kV deuterium neutral beams. The relatively low magnetic field and high beam voltage result in a population of super-Alfvénic fast ions (ions with velocity greater than the Alfvén speed), much as is expected for many fusion reactor concepts where the fusion-generated $\alpha$'s will be super-Alfvénic. A wide range of instabilities excited by the fast-ion population from neutral beam heating has been seen on NSTX [2–15], and other low aspect ratio tokamaks such as MAST [16–21] and START [22, 23].

Instabilities excited by the fast-ion population in NSTX extend from low-frequency energetic particle modes (EPMs) at tens of kHz [24–27] through beta-induced Alfvén acoustic eigenmodes (BAAE) [28–30] and toroidal Alfvén eigenmodes (TAEs), 50 to 200 kHz [2–11], up to global and compressional Alfvén eigenmodes (GAE and CAE) in the frequency range 0.3–2.5 MHz, or roughly $0.1\omega_{ci}$ to $0.7\omega_{ci}$ [31–43]. Fast-ion driven instabilities on NSTX can exhibit bursting, frequency chirping (up and/or down) and avalanching (a slow build-up in amplitude culminating in a final, rapid growth of one or more modes followed by a quiescent period [6, 8, 11, 44–46]).

GAE and CAE are of interest for their possible roles in anomalous transport of fast ions, enhancement of electron thermal diffusivity [47, 48], 'alpha-channelling' [49–52], or stochastic heating of thermal ions [53–64]. The Doppler-shifted cyclotron resonance allows the modes to extract perpendicular energy from the fast ions, possibly enhancing fast-ion confinement. The trapped-electron bounce frequency can be comparable to the GAE and CAE frequencies, resulting in the potential for resonantly enhanced trapped-electron transport. Stochastic heating of the thermal ions by large amplitude, sub-cyclotron-frequency waves has been extensively investigated theoretically ([53–58] and references

 

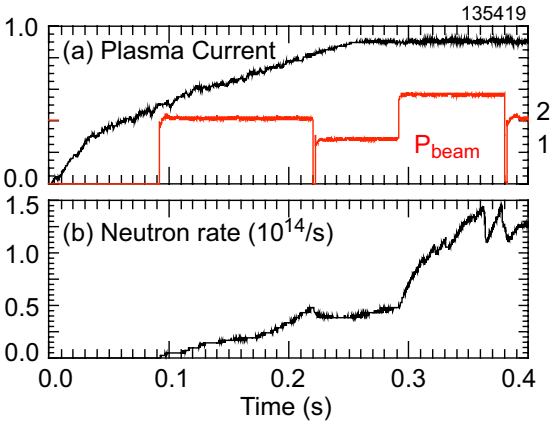


**Figure 1.** (*a*) Plasma current and heating beam power profile, (*b*) neutron rate.

therein) and experimentally [59–63], and proposed as a method for direct thermal ion heating [64]. Above the amplitude for stochastic ion heating, the waves can very efficiently transfer their energy to the thermal ion population, and the stochastic heating mechanism would tend to clamp the mode amplitude near the stochastic heating threshold. The avalanche mechanism can result in mode bursts with amplitudes much greater than the normal quasi-linear saturation amplitude, thus give the best chance for beam driven modes to exceed stochastic thresholds for thermal ion heating or trapped-electron transport. Experimental measurements of the dynamics of mode amplitude and structure evolution are thus of interest.

GAE are seen in most NSTX beam heated plasmas, but GAE avalanches are less common. The plasma current, beam heating profile in time and neutron rate from a representative shot with GAE avalanches are shown in figure 1. The time history of beam voltage and power was optimized to excite TAE avalanches, and both TAE and GAE avalanching behaviour is present. In this discharge, the GAE avalanches began around 0.23 s and continued until ≈0.38 s. The first TAE avalanche happened at ≈0.31 s. The last, at ≈0.38 s, triggered continuous $n = 1$ activity. The avalanching activity may be suppressed after 0.38 s due to an increase in density, the evolution of the $q$-profile, or redistribution of fast ions by the low-frequency $n = 1$ mode.

In the rest of the paper, section 2 will present measurements of the GAE, beginning with basic measurements of the mode wavelengths, internal structure and amplitude. The evidence for fast-ion redistribution will be presented, followed by a discussion evidence for three-wave coupling of TAE and kinks, but not involving GAE. Section 3 will discuss the physics and issues relating to the resonant destabilization of the GAE and some implications of the observed mode amplitudes.

## 2. Experimental observations

The diagnostics on NSTX with the bandwidth and sensitivity to study modes in the MHz frequency range, for this shot, include the Mirnov coil arrays (for detection and measurement of poloidal and toroidal wavelengths) and the reflectometer arrays [65] (for measurement of the internal mode amplitude

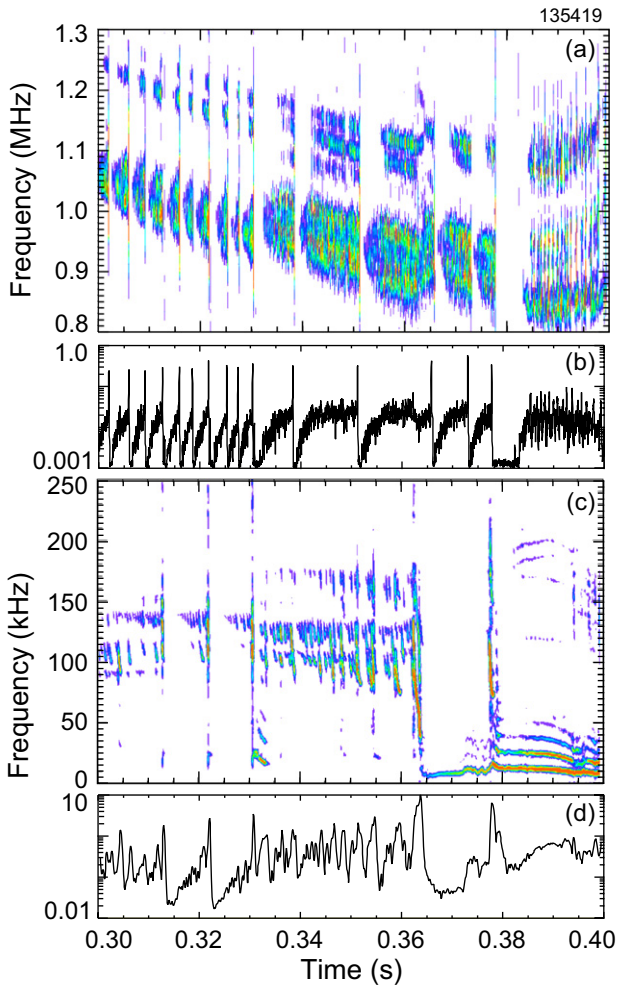


**Figure 2.** (*a*) Spectrogram showing GAEs, (*b*) rms magnetic fluctuations 0.8 MHz < freq < 1.3 MHz, (*c*) spectrogram showing TAE and low-frequency kink activity, (*d*) rms magnetic fluctuations from 30 kHz < freq < 200 kHz.

and radial structure). The reflectometers provide the only measurement of internal mode structure and amplitude for the experiments described here, but their use constrained the plasmas being studied to those with peaked density profiles (L-mode), ideally with a peak density on axis of a little more than $\approx 3.1 \times 10^{19}$ m$^{-3}$, the cut-off density of the highest frequency reflectometer channel at this time. For the 2010 campaign, a beam emission spectroscopy (BES) diagnostic [66, 67] was added with the requisite bandwidth and sensitivity to detect GAEs, and the reflectometer array was upgraded to 16 channels with the density cut-off for the highest frequency channel extended to $7 \times 10^{19}$ m$^{-3}$.

GAE and TAE avalanches detected with a Mirnov coil are shown in figure 2. The spectrogram in figure 2(*a*) and rms fluctuation level in figure 2(*b*) show GAE avalanches in an L-mode plasma. Similarly, figures 2(*c*) and (*d*) show a spectrogram with five TAE avalanches, and the rms fluctuations in the TAE-frequency band, respectively. The last TAE avalanche in these figures triggers a 'saturated fishbone', that is, an $n = 1$ kink mode that chirps down in frequency, but rather than decaying away, remains at nearly constant amplitude and frequency. This mode is likely the same as the 'long-lived' modes reported on MAST [21, 68].

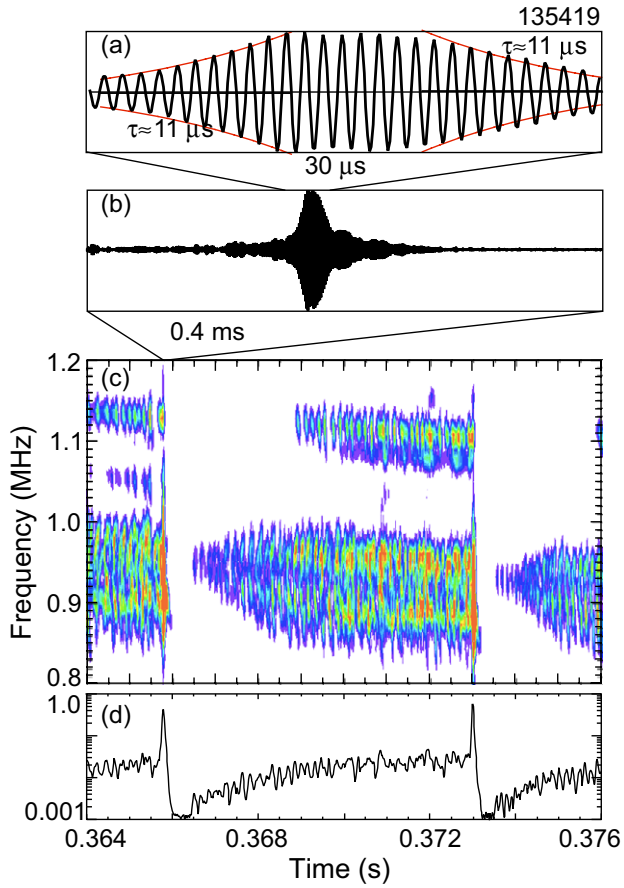


**Figure 3.** GAE avalanche burst measured with reflectometer with (*a*) growth and decay rates of $\approx 0.9 \times 10^5\ s^{-1}$ indicated, (*b*) same data, longer time period. Mirnov coil data over GAE avalanche cycle (*c*) spectrogram, (*d*) rms amplitude evolution (Gauss) on semi-logarithmic scale.

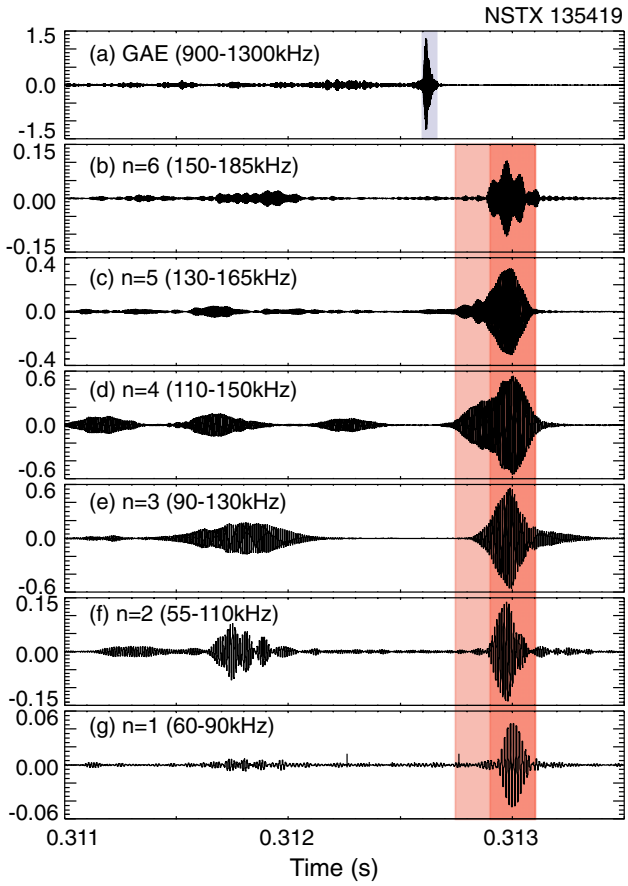


**Figure 4.** Digitally filtered Mirnov coil signal showing (*a*) GAE band, (*b*) through (*g*) the $n = 6$ through $n = 1$ TAE avalanche components, respectively. Pink indicates pre-avalanche phase, red indicates avalanche phase.

The GAE avalanche period starts off short, about 3 ms, but after 0.33 s lengthens to about 15 ms. The GAE amplitude increases exponentially for several milliseconds after each avalanche (that is a linear increase in the semi-logarithmic plot, figure 2(*b*)), reaching nearly the same amplitude in each of the avalanche periods before the rapid growth of the final burst is triggered. This two-stage growth process provides strong evidence of avalanche behaviour. In the latter, longer avalanche periods, the mode amplitude nearly saturates at a level below the apparent threshold for rapid growth. There is a period of saturation or much slower growth following the initial linear growth leading up to the rapid growth, or avalanche, phase. The peak amplitude of the final avalanche bursts, which appear as spikes in the rms plot (figure 2(*b*)), is relatively constant for the 15 avalanches seen in figures 2(*a*) and (*b*).

The spectrogram in figure 3(*c*) shows one of the later GAE avalanche cycles from ≈0.366 s to ≈0.373 s. The pre-avalanche fluctuations are seen to be an almost turbulent spectrum of fluctuations in a frequency band about 100 kHz to 150 kHz wide. These fluctuations are a mix of toroidal mode numbers, ranging from $n = 7$ to $n = 11$ (all counter propagating to the neutral beams). The rms fluctuation amplitude is shown in figure 3(*d*) on a semi-logarithmic scale. The GAE amplitude nearly saturates before the final jump in mode amplitude by an order of magnitude at the end of the avalanche cycle. In figure 3(*b*) a trace of the phase fluctuations from a quadrature reflectometer signal showing the final, large burst is shown, which is further expanded in figure 3(*a*), where growth and decay times of ≈11 $\mu$s are seen. The final large burst consists of only several tens of wave cycles near the peak amplitude.

The TAE and the GAE appear in a sequence of repetitive, short bursts where the mode grows, saturates and then decays as seen, for example, in figure 4. The amplitude at which the mode saturates depends on details of the fast-ion distribution function, and upon the equilibrium parameters, particularly the $q$-profile, density profile and to a lesser extent the temperature, which affects damping. The saturation amplitude is also affected in a complicated way by the perturbations to the fast-ion distribution by other modes. The larger the mode grows, the more fast ions become trapped in the wave in one or more 'phase-space islands' of resonant ions for each mode, changing the fast-ion distribution function and affecting the stability of other modes. If the amplitudes of one or more modes becomes sufficiently large, previously separate phase-space islands may overlap, resulting in even larger perturbations to the fast-ion distribution function. This can result in stronger growth, the triggering of additional modes and a broader relaxation of the fast-ion distribution function, that is an avalanche.

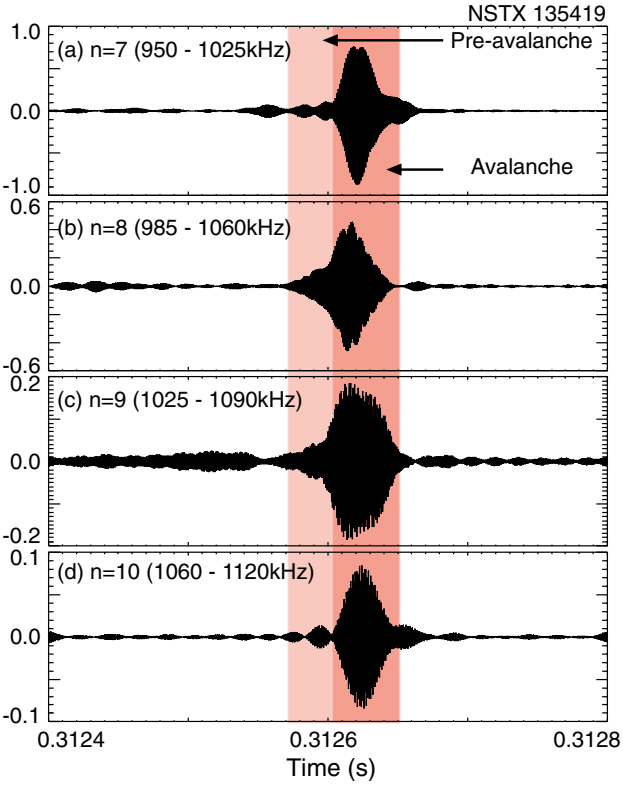


**Figure 5.** Digitally filtered Mirnov coil signal showing the dominant components of the GAE avalanche, (*a*)–(*d*) show $n = 7$ through 10, respectively.

In figure 4 are shown the dominant modes in a TAE avalanche. The figure was created by separating the even-$n$ and odd-$n$ components by spatial filtering, then separately frequency filtering the even-$n$ and odd-$n$ signals. Filtering the even-$n$ and odd-$n$ components separately allows a broader bandpass frequency range before overlapping modes nearby in frequency, thus improved time resolution of the mode amplitude evolution. In the lightly shaded pre-avalanche time range the $n = 4$ and $n = 5$ modes begin to grow, and later the $n = 3$. Just before the onset of the avalanche, the $n = 4$ and $n = 5$ modes are nearly saturated. In the more darkly shaded avalanche region, all of the modes, from $n = 1$ to $n = 6$, show strong growth, consistent with the avalanche model. Similar data are shown in figure 5 for a GAE avalanche. Here, the four strongest modes are shown. The avalanche period is much shorter for the GAE avalanche, and the relative frequency spacing is smaller. The restricted bandpass frequency range due to closely spaced modes (in frequency) compromises the time resolution of the amplitude evolution, introducing uncertainty in the timing of the onset of strong growth. Nevertheless, in this case it also appears that there is a pre-avalanche period where the $n = 8$ and $n = 9$ modes are growing, and an avalanche period where all of the modes from $n = 7$ to $n = 10$ begin much faster growth.

### 2.1. Structure of GAE

The toroidal mode number and polarization of the magnetic fluctuations are measured with a toroidal array of eight Mirnov coils, six oriented to measure the poloidal component and two oriented to measure the toroidal component of the magnetic fluctuations (figure 6). As an example, the best fit to the toroidal mode number of the dominant spectral peak of the magnetic fluctuations in the final burst in a later avalanche (0.366 s) is $n = 7$ (as it is in the other avalanches). However, decomposing the signal into the $n =$ 'odd' and $n =$ 'even' components demonstrates that there is a significant even component to the mode, and an additional $n = 7 \pm 2$ component may be inferred from the amplitude modulation of the $n =$ 'odd' component. The mode is mostly compressional at the plasma edge; the dominant magnetic perturbation is larger parallel to the equilibrium magnetic field than in the transverse direction.

The amplitude evolution and radial profile are measured with a five-channel reflectometer system. The displacement profile obtained from the reflectometer array data is shown in figure 7(*a*). The red squares are the phase fluctuation amplitudes from the quadrature reflectometer channels, converted by the free-space wavelength to an effective displacement. The blue curve, figure 7(*a*), is the effective displacement of the equilibrium density profile (that is assuming shear polarization for the wave with no compressional terms) needed to reproduce the observed reflectometer data (red curve, figure 7(*a*)). The solid black curve, figure 7(*c*), is the density perturbation, correcting for interferometric contributions, inferred from the reflectometer data, independent of the shear or compressional nature of the wave. The inferred density perturbation is multiplied by 50 (solid black curve) to be visible in this figure, and the peak perturbed density is $\delta n/n \approx 1\%$. The relative phases of the density fluctuations measured by the five channels are shown in figure 7(*b*). The $q$-profiles deduced from equilibrium reconstructions constrained with MSE data, starting 20 ms after the GAE burst when MSE data becomes available, are shown in figure 7(*d*). The mode amplitude appears to peak near or inside of $q_{\min}$.

### 2.2. GAE induced fast-ion transport

Neutron rate drops, or evidence of fast-ion redistribution or loss in the fast-ion D-alpha (FIDA) [69] or scintillator fast lost ion probe (sFLIP) [70] data, are not seen to correlate with the GAE avalanches. Indeed, as the cyclotron resonance is presumed to take primarily perpendicular energy from the fast ions, reducing the radial excursion (larmor radius and banana orbit width), these modes may actually improve their confinement. However, the GAE-quiescent period following each strong burst is consistent with a fast-ion redistribution which reduces the free-energy available to drive the modes. Additional indirect evidence of fast-ion redistribution is shown in figure 8, where the rms fluctuation levels for GAE (red) and TAE (blue) are shown. The three TAE avalanche events in this time range, at 0.313, 0.322 and 0.331 s, are seen as spikes in the blue curve. A GAE avalanche precedes each of the three TAE avalanches by several hundred microseconds, although not every GAE avalanche is followed by a corresponding TAE avalanche. The timing suggests that the redistribution of fast ions from the GAE avalanche provided some of the impetus to trigger the TAE avalanche.

A database was compiled of the timing of 358 GAE avalanches and 51 TAE avalanches in shots where GAE and

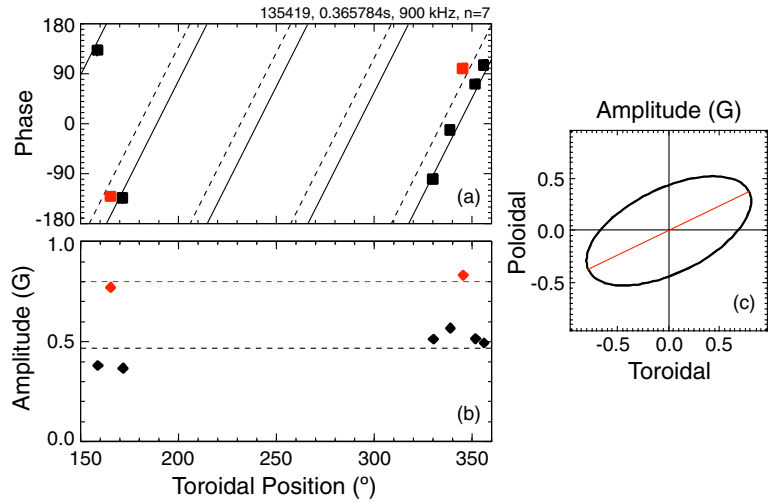


**Figure 6.** (*a*) Relative phase data from Mirnov coil array. Red points are toroidally oriented coils, black poloidal, (*b*) fluctuation amplitude in Gauss, (*c*) composite Lissajous figure based on amplitude and phase data.

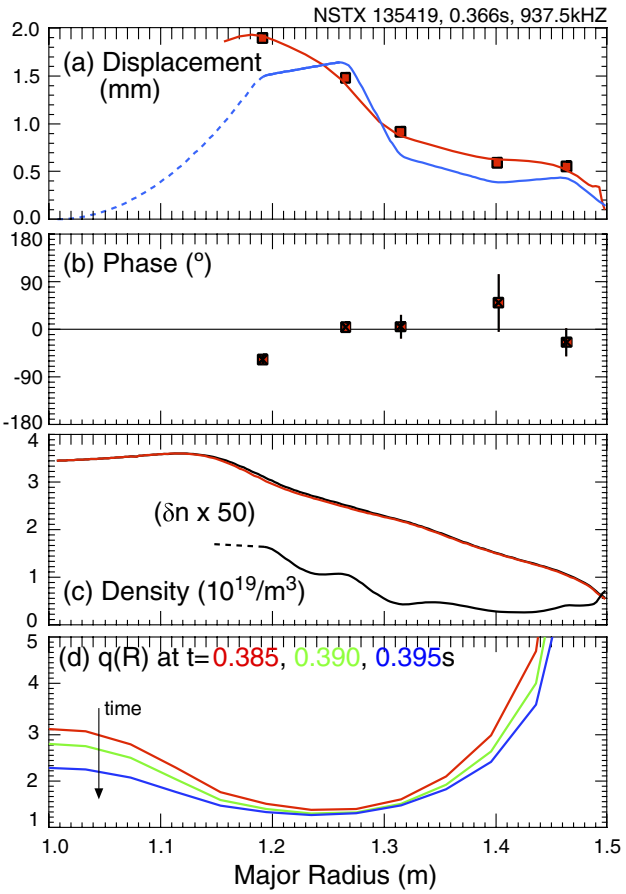


**Figure 7.** (*a*) Mode amplitude profile from reflectometer array, (*b*) relative phase of mode, (*c*) density profile, (*d*) $q$-profile from equilibrium reconstruction with MSE pitch-angle data.

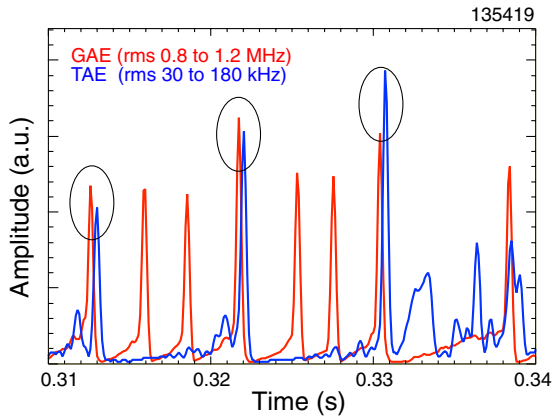


**Figure 8.** RMS fluctuation levels in GAE frequency band (red) and TAE-frequency band (blue). Relative fluctuation amplitudes between red/blue curves is arbitrary; shown for timing only.

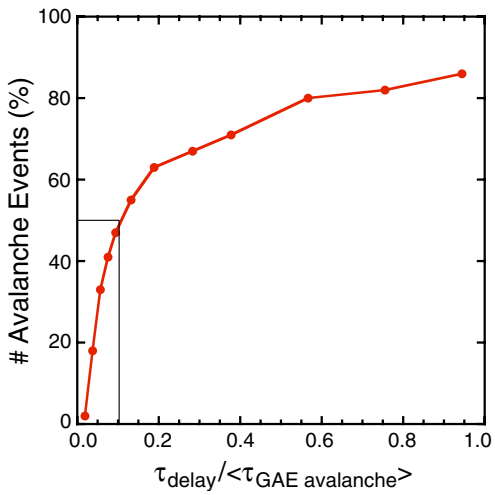


**Figure 9.** Per cent of TAE avalanche events occurring in the time interval following a GAE avalanche, normalized to the average TAE avalanche period.

TAE avalanches co-existed. From figure 9 it is seen that 50% of the TAE avalanches occur within the first 10% of the GAE avalanche cycle. If the timing of the TAE avalanches were not correlated with the GAE avalanches, the curve would be approximately linear, with ≈10% of the TAE avalanches in the first 10% of the GAE avalanche cycle. The occurrence of the

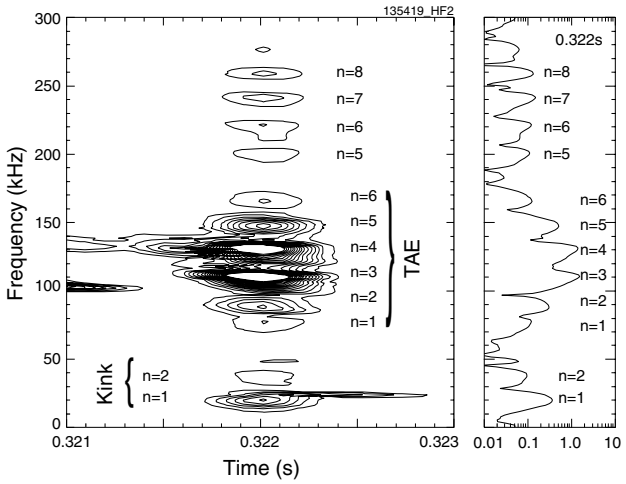


**Figure 10.** Spectrogram of Mirnov coil signal showing (*a*) multiple modes with toroidal mode numbers identified, (*b*) spectrum at 0.322 s on logarithmic scale.

TAE avalanches shortly after the GAE avalanche suggests a causal relation.

### *2.3. Three-wave coupling in TAE, not GAE*

The correlation of the TAE and GAE avalanches is most likely to occur through changes to the fast-ion distribution; however, three-wave coupling of TAE to a much lower frequency kink (and higher frequency modes) has been previously observed on NSTX [7, 71]. As is seen below, there is no apparent wave-wave coupling of the GAE and TAE, leaving modifications to the fast-ion distribution as the most likely candidate for the triggering of the TAE avalanches by the GAE.

A spectrogram of the TAE avalanche at 0.322 s is shown in figure 10. There are $n = 1$ through $n = 6$ TAE in the final TAE avalanche burst, with the two dominant modes being the $n = 3$ and $n = 4$. The modes are approximately evenly spaced in frequency, within the ±3 kHz accuracy resulting from the short, ≈0.2 ms, period of the final TAE avalanche burst. A second group of modes in a frequency band 180 kHz to 300 kHz have mode numbers and frequencies which satisfy the non-linear mode coupling relations that $f_3 = f_1 + f_2$ and $n_3 = n_1 + n_2$ for the TAEs in the frequency range 70–180 kHz. For example, the frequency of the $n = 7$ mode at 240 kHz is, within measurement accuracy, the sum of either of the $n = 3$ and $n = 4$, the $n = 2$ and $n = 5$ or the $n = 1$ and $n = 6$ mode frequencies. Similarly, the $n = 1$ mode at ≈20 kHz is consistent with the difference frequency of the $n = 4$ and $n = 3$ modes [7, 71].

The Mirnov signal through the GAE and TAE bursts is shown in more detail in figure 11. The Mirnov coil signal is digitally filtered into four frequency bands. The GAE avalanche burst is seen in the frequency band from 0.8 to 1.2 MHz (figure 11(*a*)) and the TAE avalanche burst in the range from 60 to 180 kHz (figure 11(*c*)). It is clear that the GAE burst precedes the onset of the TAE avalanche. The amplitude modulation of the TAE-frequency fluctuations is due to the beating of the dominant, nearly equal amplitude $n = 3$ and $n = 4$ modes. Figures 11(*b*) and (*d*) show the digitally filtered

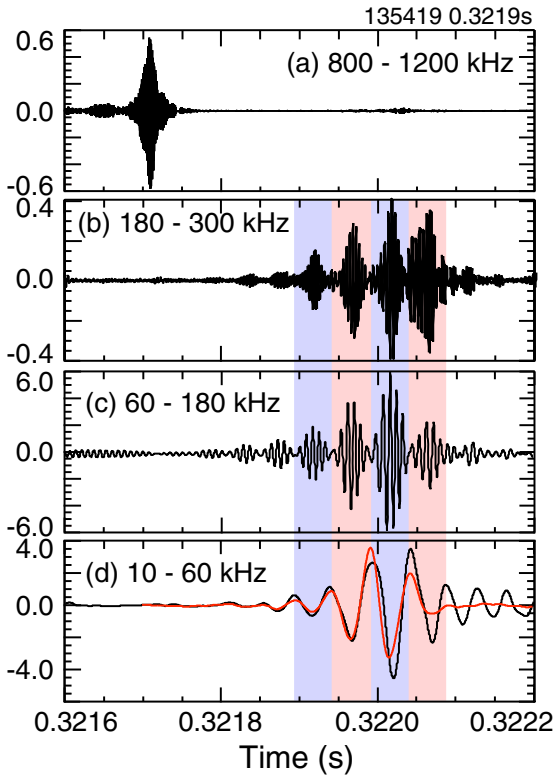


**Figure 11.** Mirnov coil digitally bandpass filtered in three ranges showing (*a*) GAE burst, (*b*) TAE-frequency doubling, (*c*) TAE avalanche and (*d*) $n = 1$ internal kink, red curve is a simulation of non-linear coupling, scaled to match the kink.

signal for the frequency bands covering the sum and difference frequencies of the TAEs.

The non-linear coupling of the low- and high-frequency bursts can be simulated by squaring the bandpass-filtered TAE fluctuations (figure 9(*c*)), and again filtering the result to separate the 20 kHz component. This is shown in figure 9(*d*) where the red curve is the simulated non-linear coupling, inverted and scaled to match the measured $n = 1$ mode amplitude [7, 71]. The simulated and experimental signals initially track well, but later diverge, suggesting that an independent $n = 1$ mode was excited at the difference frequency, which then decayed when the non-linear drive from the TAE burst was gone.

In figure 12 the GAE burst of figure 11(*a*) is shown on an expanded timescale. Here the magnetic fluctuations as measured with two coils separated by 180° in the toroidal direction (figures 12(*a*) and (*b*)) are separated into the odd-*n* and even-*n* components (figures 12(*c*) and (*d*)). The odd component still shows evidence of beating in the amplitude evolution, consistent with an additional odd toroidal mode of smaller amplitude. The even component is somewhat weaker, also with possibly some weak beating. The difference frequency is about 100 kHz, as estimated by the beat period in figures 12(*c*) and (*d*). This is roughly equal to the TAE frequency, but apparently is not a non-linear three-wave coupling with the TAE as the TAE amplitude is small at this time (figures 11(*a*) and (*c*)). Further, the mode number difference for the GAE is 1 or 2, whereas the dominant TAE activity is $n = 3$ and $n = 4$. Thus, it appears that the GAE

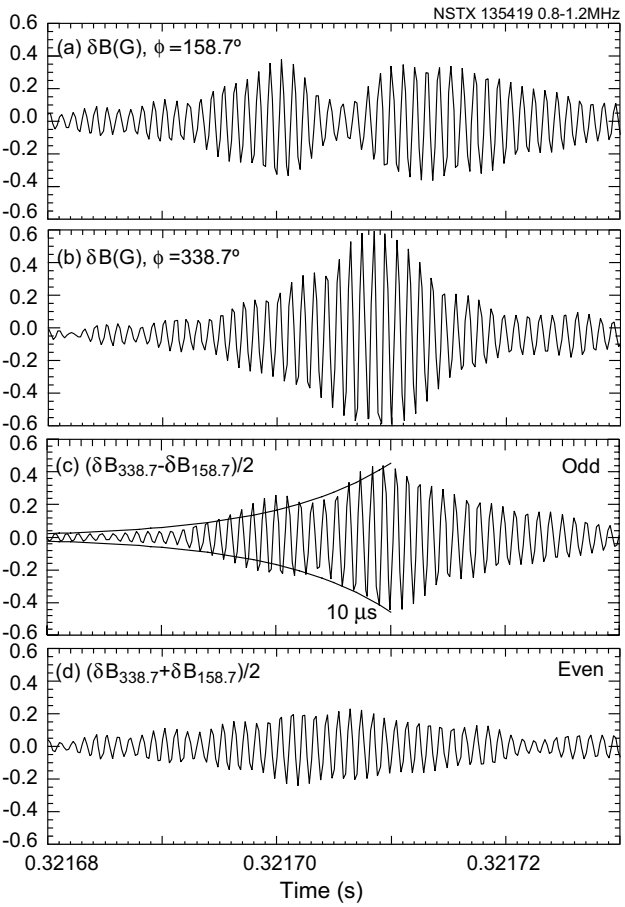


**Figure 12.** (*a*) Digitally filtered Mirnov coil signal from toroidal angle of 171.5°, (*b*) similar from 351.5°, (*c*) odd component of final GAE avalanche burst with growth rates of $10^5\ s^{-1}$ and $2 \times 10^5\ s^{-1}$ indicated, (*d*) even component (from Mirnov coils).

avalanche burst does not exhibit strong non-linear coupling to the TAE, but rather involves two or more nearly independent modes.

## 3. Discussion and analysis

These observations of GAE activity are relevant to the physics of fast-ion avalanches, stochastic ion heating, alpha-channelling and fast-ion redistribution. In this section, the measurements of mode structure and mode amplitude evolutions are examined with respect to these various areas of fast particle driven mode physics. But first, the identification of the modes and the resonant drive for the modes is discussed.

The profile of the internal density fluctuation is measured with the reflectometer array, and the magnetic fluctuations are measured externally with Mirnov coils. There are no reflectometer measurements for $R < 1.2$ m, but these data indicate that the density fluctuations peak near or inside the region of $q_{\min}$. This would be consistent with identification of these modes as GAE, rather than CAE, which should have had a peak in amplitude further out. The pitch of the magnetic field perturbation measured at the plasma wall indicates that the mode has some compressional component, whereas GAEs are in principal shear Alfvén waves. However, toroidicity, magnetic shear and finite beta are observed to

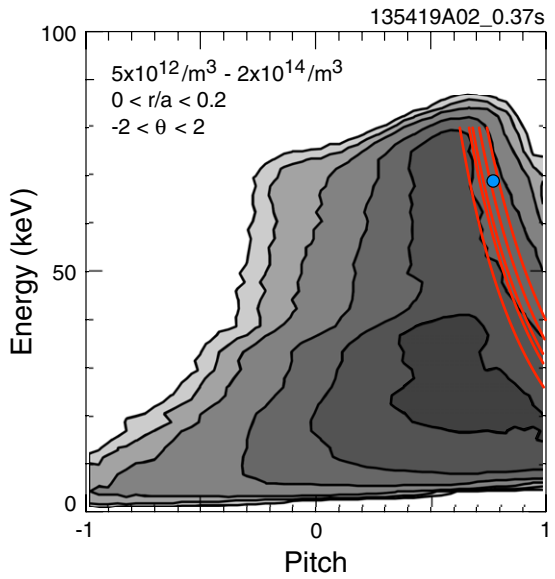


**Figure 13.** Distribution function calculated with the TRANSP beam deposition code. Red curves indicate fast ions resonant with the five dominant modes. The blue point indicates pitch and energy of particle whose trajectory is shown in figure 14.

introduce compressional components in numerical simulations of GAE for NSTX parameters [42], thus edge polarization measurements are inconclusive regarding mode identification.

The pitch of fast ions resonant with the mode can be estimated from the local GAE dispersion relation $\omega = k_\parallel V_{\text{Alfvén}}$ and the Doppler-shifted cyclotron resonance condition, $\omega = \omega_{\text{ci}} - k_\parallel V_{b\parallel}$. The GAE dispersion relation is used to estimate $k_\parallel$ from the mode frequency in the plasma frame and the local Alfvén velocity. The resonant pitch is then $V_{b\parallel}/V_b = (\omega_{\text{ci}} - \omega)/\omega(V_{\text{Alfvén}}/V_b)$. For the dominant modes in the avalanche burst, this gives a range of pitches for the resonant 80 keV fast ions of $0.65 < V_{b\parallel}/V_b < 0.8$. As the ion energy drops, the pitch required for resonance increases, that is the parallel energy remains constant to satisfy the resonance condition, but the perpendicular energy can be lower, resulting in higher pitch.

The fast-ion distribution function calculated in TRANSP is shown in figure 13 and the resonant conditions as a function of energy for the five largest modes are indicated by the red lines. The resonance curve sits on the side of a 'bump-on-tail' in perpendicular energy, but a more comprehensive analysis of the stability and resonant drive physics are beyond the scope of this paper. Numerical simulations have been done [42] and an analytic model of the Doppler-shifted cyclotron resonance instability has been developed [72].

One challenge for analytic models of the Doppler-shifted cyclotron resonance in low aspect ratio plasmas is that the orbits of most fast ions move over a wide range of magnetic field strengths, and thus the cyclotron frequency changes significantly over the orbit. As the resonance with the mode, $\omega_{\text{ci}} - k_\parallel V_{b\parallel} = \omega_{\text{mode}}$, depends on the cyclotron frequency, fast ions will move into and out of resonance on a timescale short compared with a wave period. However, a numerical simulation of GAE with the initial value code, HYM, has been able to demonstrate instability of both GAE and CAE through the Doppler-shifted cyclotron resonance drive. The

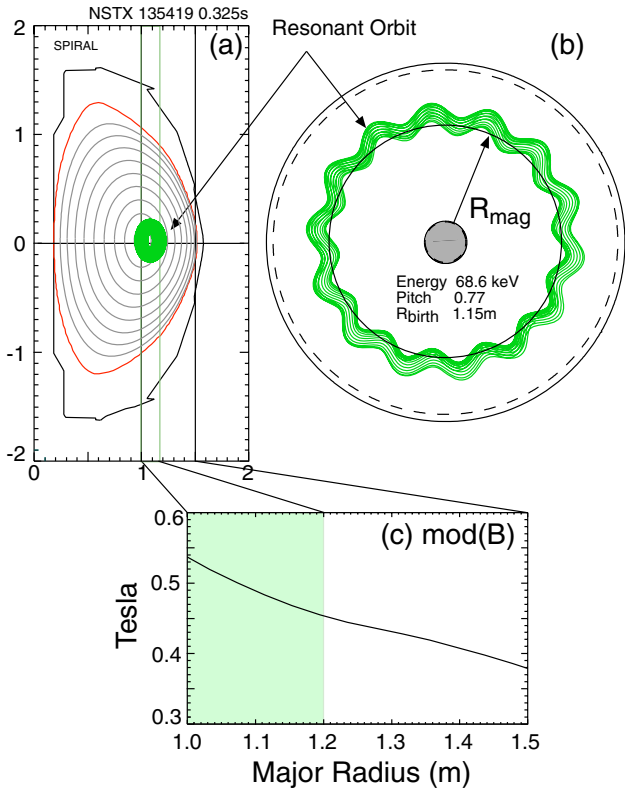


**Figure 14.** Orbit of a representative fast ion resonant with the GAE, (*a*) mapped to the poloidal cross-section, (*b*) plan view and (*c*) mod($B$) on midplane with shaded region showing the range of the guiding centre.

typical fast ions resonant with the GAE in the HYM simulation have passing orbits constrained to the outboard midplane. An example orbit calculated with the SPIRAL [73] code is mapped to a poloidal cross-section as shown in figure 14. The radial extent of the orbit guiding centre corresponds to a variation in cyclotron frequency of only ±5%, or a frequency modulation amplitude of ≈200 kHz (out of $\langle f_{\rm ci}\rangle \approx 3.9$ MHz). There are approximately 16 gyro-periods in each poloidal transit, or $f_{\rm pol} \approx 3.9\,{\rm MHz}/16 \approx 245$ kHz. In the resonant fast-ion frame, the mode frequency is Doppler-shifted to match the cyclotron frequency, as noted previously ($\omega + k_\parallel V_{b\parallel} = \omega_{\rm ci}$). The relative phase variation between the mode and the cyclotron gyrations over a poloidal transit can be estimated by integrating the approximate modulation of the cyclotron frequency and parallel velocity. The approximate formula for the phase variation is

$$\delta\phi(t) \approx \frac{\langle k_\parallel V_{b\parallel}\rangle}{\omega_{\rm T}}\frac{\varepsilon}{2}\frac{1-p^2}{p^2}\sin(\omega_{\rm T}t) + \frac{\langle\omega_{\rm ci}\rangle}{\omega_{\rm T}}\varepsilon\sin(\omega_{\rm T}t).$$

Here, $p$ is the particle pitch, $\omega_{\rm T}$ is the transit frequency and $\varepsilon$ is the inverse aspect ratio. The first term (r.h.s.) is from the modulation of the parallel velocity, the second is from the modulation of the cyclotron frequency. For the fast-ion parameters shown in figure 14, the amplitude of the phase modulation over a poloidal transit is ≈65°; probably large enough to affect the mode drive and the fast-ion trapping, but probably not large enough to destroy the resonance.

The early GAE amplitude evolution is suggestive of avalanching behaviour, with a slow growth in mode amplitude as the fast-ion population builds up, leading to a short, explosive growth to much larger amplitude which is then followed by a quiescent period. After 0.33 s, however, the slow growth seems to saturate for an extensive period of time. This could be explained if the mode amplitude saturated just below the threshold for triggering an avalanche. An intriguing alternative explanation is that this represents the 'stochastic thermal ion heating' threshold. At this amplitude, there is an effective damping term increasing strongly with mode amplitude as the wave dumps energy into the thermal ion population. In the 'linear' regime, the mode drive is fixed or falling with mode amplitude and this quickly leads to saturation. The potential effective heating power is estimated below, but depending upon how far below the 'natural' saturation amplitude the stochastic threshold is, a still substantial portion of the power will go to the electrons through Landau damping.

The presence of multiple modes in the final, large bursts, is indicated by the amplitude modulations of the even and odd signals. The presence of the multiple modes complicates the measurement of the growth and damping rates in the final burst. However, the observed growth and decay of the final bursts appears roughly symmetrical, with growth and damping times of approximately 10 $\mu$s, or $\gamma/\omega \approx 3.4\%$. If the assumption is made that the drive is negligible during the burst decay, figure 3(*a*) suggests that the peak drive, $\gamma_{\rm drive}$, is approximately twice the damping rate, $\gamma_{\rm damp}$, e.g. $\gamma_{\rm growth} = \gamma_{\rm drive} - \gamma_{\rm damp} \approx \gamma_{\rm damp} \approx 10^5\ {\rm s}^{-1}$.

The peak mode amplitude of $\delta n/n \approx 1\%$ can be used to estimate the magnetic fluctuation level, which together with the growth/damping rate estimate can be used to estimate the power flow from the fast-ion population through the mode and into the thermal plasma. For compressional modes, the relation is $\delta B/B \approx \delta n/n$, for shear modes, the relation is more complicated, but roughly $\delta B/B \approx L_n/L_B\delta n/n$, where $L_B$ is the relevant magnetic gradient scale length. As the magnetic gradient scale length is typically greater than the density gradient scale length, the magnetic perturbations for shear waves would generally be weaker, for a given density perturbation, than for compressional waves. In the following discussion, we use the larger estimate for magnetic fluctuations from the compressional approximation to give an upper estimate for energy in the mode. The peak amplitude of $\delta n/n \approx 1\%$ implies $\delta B/B \leqslant 1\%$ or $\delta B \approx 40$ G.

The total energy density in the wave may be estimated as twice $4\times10^{-3}\,{\rm J\,m^{-3}\,G^{-2}}\,(40\,{\rm G})^2 \approx 13\,{\rm J\,m^{-3}}$. The wave amplitude is small outside of $R \approx 1.3$ m, thus the plasma volume where mode amplitude is significant is ≈3.2 m$^3$, and the peak wave energy is ≈40 J. These estimates are very approximate, but suggest that ≈40 J of energy is transferred from the fast-ion population to the thermal plasma at each GAE avalanche event. The ten avalanche events between 0.3 and 0.33 s give an average heating power of ≈13 kW. The peak heating power from the pre-avalanche phase, assuming an effective damping rate of $10^5\ {\rm s}^{-1}$, and roughly 10% of the amplitude reached during the avalanche, is ≈50 kW, although the time average would be much less. Much of this power, of course, goes to the electrons through electron Landau damping.

The estimated peak density fluctuation level reaches $\delta n/n$ of approximately 1%; a level which might exceed the threshold

for stochastic heating of thermal ions or transport of trapped electrons. Simulations of thermal ion heating were performed with a fixed spectrum of 20 modes, each with amplitude of $\delta B/B \approx 0.13\%$, or $20^{1/2}\delta B/B \approx 0.6\%$, gave heating rates of up to 50 eV ms$^{-1}$ in perpendicular energy, and 17 eV ms$^{-1}$ in parallel energy [74]. The estimated peak GAE amplitude of $\delta B_{\rm rms}/B \approx 1\%$ during the avalanche burst is comparable, albeit comprised of an unknown number of modes. The heating rate increases non-linearly with mode amplitude, but the typical burst duration of $\approx 20\,\mu$s would result in a thermal temperature rise of $<1$ eV per GAE avalanche. Using the same formalism as above with an ion density of $2.4 \times 10^{19}$ m$^{-3}$ predicts a net increment to the ion thermal energy of $\approx 4$ J, compared with the estimate of 40 J of heating made above. The thermal ion heating at the pre-avalanche level of 10% of the avalanche peak amplitude, or 0.02%, is predicted to result in negligible heating of the thermal ions. Stochastic ion heating may play a role in limiting the peak amplitude of the avalanche, but appears to play a negligible role in the thermal ion power balance.

A broad spectrum of GAE activity has also been implicated in enhanced electron thermal transport [47], most often correlated with a flattening of the electron temperature profile in the core. Such flattening is associated with density fluctuation amplitudes of $\delta n/n \approx 0.1\%$, which is comparable to the pre-avalanche level, and much less than the peak amplitude of $\delta n/n \approx 1\%$. Whether this interaction with the thermal electrons can provide some additional drive for the GAE, and how this affects the avalanche model, will be the object of further research.

## 4. Summary

A broad spectrum of modes in the frequency range from 0.5 to 1.5 MHz is often seen in NSTX beam heated plasmas. The modes are surmised to be global Alfvén eigenmodes based on their spectrum and evolution of frequencies. The GAEs are expected to be localized near the low-shear region of minimum $q$. Internal measurements show modes are indeed peaked towards the magnetic axis, possibly near the off-axis minimum in $q$. The peak mode amplitude as measured with the reflectometers reaches $\delta n/n \approx 1\%$. The modes exhibit a range of behaviour, including chirping, bursting as well as more continuous activity. In this paper we have presented data documenting behaviour characterized as avalanching, a slow growth in mode amplitude following a quiescent period, culminating in very rapid growth of multiple modes leading again to a quiescent period. The avalanches are seen to involve multiple modes with toroidal mode numbers from roughly $n = 7$ to $n = 11$.

The modes are postulated to be excited through a Doppler-shifted cyclotron resonance with beam ions, an assumption supported by numerical simulations. We have estimated the energy dependence on pitch-angle for fast ions satisfying this resonance condition and have shown that it aligns well with the distribution of fast ions calculated with the TRANSP code. We deduce that these avalanches redistribute fast ions from the quiescent period following the avalanche burst and by the apparent triggering of TAE avalanches at lower frequency. So far, direct measurements of fast-ion population have been insufficiently sensitive to detect this implied redistribution. However, the cyclotron resonance is predicted to reduce the perpendicular energy of fast ions, making their radial excursions from there flux surface smaller. Thus, the GAE could hypothetically improve the fast-ion confinement.

## Acknowledgments

This manuscript has been authored by Princeton University under Contract Numbers DE-AC02-09CH11466 and DE-FG03-99ER54527 with the US Department of Energy.

## References

[1] Ono M. *et al* and the NSTX Team 2000 *Nucl. Fusion* **40** 557
[2] Gorelenkov N.N., Cheng C.Z., Fu G.Y., Kaye S. and White R. 2000 *Phys. Plasmas* **7** 1433
[3] Fredrickson E.D. *et al* 2003 *Phys. Plasmas* **10** 2852
[4] Heidbrink W.W., Fredrickson E., Gorelenkov N.N., Hyatt A.W., Kramer G. and Luo Y. 2003 *Plasma Phys. Control. Fusion* **45** 983
[5] Fredrickson E.D. *et al* 2006 *Phys. Plasmas* **13** 056109
[6] Fredrickson E.D., Gorelenkov N.N., Bell R.E., Menard J.E., Roquemore A.L., Kubota S., Crocker N.A. and Peebles W. 2006 *Nucl. Fusion* **46** s926
[7] Crocker N.A., Peebles W.A., Kubota S., Fredrickson E.D., Kaye S.M., LeBlanc B.P. and Menard J.E. 2006 *Phys. Rev. Lett.* **97** 045002
[8] Podestà M. *et al* 2009 *Phys. Plasmas* **16** 056104
[9] Heidbrink W.W., Ruskov E., Fredrickson E.D., Gorelenkov N., Medley S.S., Berk H.L. and Harvey R.W. 2006 *Plasma Phys. Control. Fusion* **48** 1347–72
[10] Fredrickson E.D. *et al* 2006 *Phys. Plasmas* **13** 056109
[11] Fredrickson E.D. *et al* 2009 *Phys. Plasmas* **16** 122505
[12] Fredrickson E.D., Gorelenkov N.N. and Menard J. 2004 *Phys. Plasmas* **11** 3653
[13] Fredrickson E.D., Cheng C.Z., Chen L., Darrow D., Gorelenkov N.N., Johnson D., Kaye S., Kubota S., Menard J. and White R.B. 2002 *Proc. 29th EPS Conf. on Plasma Physics and Controlled Fusion (Montreux, Switzerland, 17–21 June 2002)* vol 26B (ECA) paper P-1.104 http://epsppd.epfl.ch/Montreux/pdf/P1_104.pdf
[14] Berk H.L. *et al* and JET EFDA contributors 2006 *Proc. 21st Int. Conf. on Fusion Energy 2006 (Chengdu, China, 2006)* (Vienna: IAEA) CD-ROM file [TH/3-1] and http://www-naweb.iaea.org/napc/physics/FEC/FEC2006/html/index.htm
[15] Fredrickson E.D. *et al* 2002 *Phys. Plasmas* **9** 2069
[16] Sharapov S.E. *et al* JET-EFDA Contributors and the MAST Team 2005 *Nucl. Fusion* **45** 1168–77
[17] Sykes A. *et al* 2001 *Nucl. Fusion* **41** 1423
[18] Gryaznevich M.P. and Sharapov S.E. 2004 *Plasma Phys. Control. Fusion* **46** s15
[19] Pinches S.D., Berk H.L., Grayaznevich M.P., Sharapov S.E. and JET-EFDA Contributors 2004 *Plasma Phys. Control. Fusion* **46** S47
[20] Tournianski M.R., Akers R.J., Carolan P.G. and Keeling D.L. 2005 *Plasma Phys. Control Fusion* **47** 671
[21] Gryaznevich M.P. *et al* and the MAST Team 2008 *Nucl. Fusion* **48** 084003
[22] McClements K.G., Gryaznevich M.P., Sharapov S.E., Akers R.J., Appel L.C., Counsel G.F., Roach C.M. and Majeski R. 1999 *Plasma Phys. Contol. Fusion* **41** 661
[23] Gryaznevich M.P. and Sharapov S.E. 2000 *Nucl. Fusion* **40** 907
[24] Chen L. 1994 *Phys. Plasmas* **1** 1519
[25] Cheng C.Z., Gorelenkov N.N. and Hsu C.T. 1995 *Nucl. Fusion* **35** 1639

[26] Todo Y., Shinohara K., Takechi M. and Ishikawa M. 2003 *J. Plasma Fusion Res.* **79** 1107
[27] Fredrickson E.D., Chen L. and White R.B. 2003 *Nucl. Fusion* **43** 1258
[28] Gorelenkov N.N. *et al* 2007 *Plasma Phys. Control. Fusion* **49** B371–83
[29] Gorelenkov N.N., Van Zeeland M.A., Berk H.L., Crocker N.A., Darrow D., Fredrickson E., Fu G.-Y., Heidbrink W.W., Menard J. and Nazikian R. 2009 *Phys. Plasmas* **16** 056107
[30] Eremin D. Yu. and Könies A. 2010 *Phys. Plasmas* **17** 0012108
[31] Gorelenkov N.N. and Cheng C.Z. 1995 *Nucl. Fusion* **35** 1743
[32] Gorelenkov N.N. and Cheng C.Z. 1995 *Phys. Plasmas* **2** 1961
[33] Gorelenkov N.N., Cheng C.Z. and Fredrickson E. 2002 *Phys. Plasmas* **9** 3483
[34] Gorelenkov N.N., Cheng C.Z., Fredrickson E., Belova E., Gates D., Kaye S., Kramer G.J., Nazikian R. and White R.B. 2002 *Nucl. Fusion* **42** 977
[35] Gorelenkov N.N., Fredrickson E., Belova E., Cheng C.Z., Gates D., Kaye S. and White R. 2003 *Nucl. Fusion* **43** 228
[36] Belova E., Gorelenkov N.N., Cheng C.Z. and Fredrickson E.D. 2003 *Proc. 30th European Physical Society Conf. on Controlled Fusion and Plasma Physics (St Petersburg, Russia, July 2003)* vol 27A (ECA) P-3.102
[37] Belikov V.S. and Kolesnichenko Ya.I. and White R.B. 2003 *Phys. Plasmas* **10** 4771
[38] Eliezer Hameiri, Akihiro Ishizawa and Akio Ishida 2005 *Phys. Plasmas* **12** 072109
[39] Heidbrink W.W., Fredrickson E.D., Gorelenkov N.N., Rhodes T.L. and Van Zeeland M.A. 2006 *Nucl. Fusion* **46** 324
[40] Ya. Kolesnichenko, White R.B. and Yakovenko Yu.V. 2006 *Phys. Plasmas* **13** 122503
[41] Belova E.V., Jardin S.C., Ji H., Yamada M. and Kulsrud R. 2000 *Phys. Plasmas* **7** 4996
[42] Belova E. 2010 Numerical modeling of NBI-driven sub-cyclotron frequency modes in NSTX*Bulletin of the American Physical Society, 52nd Annual Meeting of the Division of Plasma Physics (Chicago, IL, 8–12 November 2010)* paper TI2-3 http://meetings.aps.org/Meeting/DPP10/Event/131371
[43] Appel L.C., Fülöp T., Hole M.J., Smith H.M., Pinches S.D., Vann R.G.L. and The MAST Team 2008 *Plasma Phys. Control. Fusion* **50** 115011
[44] Berk H.L., Breizman B.N. and Pekker M. 1995 *Phys. Plasmas* **2** 3007
[45] Berk H.L., Breizman B.N. and Pekker M. 1995 *Nucl. Fusion* **35** 1713
[46] Berk H.L., Breizman B.N., Fitzpatrick J. and Wong H.V. 1995 *Nucl. Fusion* **35** 1661
[47] Stutman D., Delgado-Aparicio L., Gorelenkov N., Finkenthal M., Fredrickson E., Kaye S., Mazzucato E. and Tritz K. 2009 *Phys. Rev. Lett.* **102** 115002
[48] Kolesnichenko Ya.I., Yakovenko Yu.V. and Lutsenko V.V. 2010 *Phys. Rev. Lett.* **104** 075001
[49] Fisch N.J. and Rax J.-R. 1992 *Phys. Rev. Lett.* **69** 612
[50] Herrmann M.C. and Fisch N. 1997 *Phys. Rev. Lett.* **79** 1495
[51] Fisch N.J., Fruchtman A., Karney C.F.F., Herrmann M.C. and Valeo E.J. 1995 *Phys. Plasmas* **6** 2375
[52] Gorelenkov N.N., Fisch N.J. and Fredrickson E. 2010 *Plasma Phys. Control. Fusion* **52** 055014
[53] Smith G.R. and Kaufman A.N. 1975 *Phys. Rev. Lett.* **34** 1613
[54] Karney C.F.F. and Bers A. 1977 *Phys. Rev. Lett.* **39** 550
[55] Karney C.F.F. 1978 *Phys. Fluids* **21** 1584
[56] Hsu J.Y., Matsuda K., Chu M.S. and Jensen T.H. 1979 *Phys. Rev. Lett.* **43** 203
[57] Drake J.F. and Lee T.T. 1981 *Phys. Fluids* **24** 1115
[58] Chen L., Lin Z. and White R. 2001 *Phys. Plasmas* **8** 4713
[59] McChesney J.M., Stern R.A. and Bellan P.M. 1987 *Phys. Rev. Lett.* **59** 1436
[60] McChesney J.M., Bellan P.M. and Stern R.A. 1991 *Phys. Fluids* B **3** 3363
[61] Bailey A.D. III, Bellan P.M. and Stern R.A. 1995 *Phys. Plasmas* **2** 2963
[62] Bailey A.D. III, Stern R.A. and Bellan P.M. 1993 *Phys. Rev. Lett.* **71** 3123
[63] Sanders S.J., Bellan P.M. and Stern R.A. 1998 *Phys. Plasmas* **5** 716
[64] Fredrickson E.D., Phillips C.K., Hosea J., Wilson J.R., Bonoli P., Gorelenkov N.N., Wright J. and Valeo E. 2007 *Radio Frequency Power In Plasmas, 17th Topical Conf. on Radio Frequency Power in Plasmas (Clearwater, FL, 7–9 May 2007) AIP Conference Proceeding* vol 933, ed P.M. Ryan and D.A. Rasmussen, Melville, New York p 111 2007 http://proceedings.aip.org/resource/2/apcpcs/93311/11_1
[65] Kubota S., Nguyen X.V., Peebles W.A., Zeng L. and Doyle E.J. 2001 *Rev. Sci. Instrum.* **72** 348
[66] Smith D.R., Feder H., Feder R., Fonck R.J., Labik G., McKee G.R., Schoenbeck N., Stratton B.C., Uzun-Kaymak I. and Winz G. 2010 *Rev. Sci. Instrum.* **81** 10D717
[67] Tritz K. *et al* and the NSTX Team 2010 *Bulletin of the American Physical Society, 52nd Annual Meeting of the Division of Plasma Physics (Chicago, IL, 8–12 November 2010)* paper PI2-2, p 238 http://meetings.aps.org/Meeting/DPP10/Event/131103
[68] Chapman I.T., M.-D. Hua, Pinches S.D., Akers R.J., Field A.R., Graves J.P., Hastie R.J., Michael C.A. and the MAST Team 2010 *Nucl. Fusion* **50** 045007
[69] Podestà M., Heidbrink W.W., Bell R.E. and Feder R. 2008 *Rev. Sci. Instrum.* **79** 10E521
[70] Darrow D.S. 2008 *Rev. Sci. Instrum.* **79** 023502
[71] Podestá M., Bell R.E., Crocker N.A., Fredrickson E.D., Gorelenkov N.N., Heidbrink W.W., Kubota S., LeBlanc B.P. and Yuh H. 2011 *Nucl. Fusion* **51** 063035
[72] Fredrickson E.D. *et al* 2010 *Proc. 23rd Int. Conf. on Fusion Energy 2010 (Daejeon, South Korea, 2010)* (Vienna: IAEA) CD-ROM file [EXW/P7-06] and http://www-naweb.iaea.org/napc/physics/FEC/FEC2010/html/index.htm
[73] Kramer G.J., White R.B., Nazikian R. and Berk H.L. 2008 Fusion-born alpha particle ripple loss studies in ITER*Proc. 22nd Int. Conf. on Fusion Energy 2008 (Geneva, Switzerland, 2008)* (Vienna: IAEA) CD-ROM file [IT/P6-3] and http://www-naweb.iaea.org/napc/physics/FEC/FEC2008/html/index.htm
[74] Gates D.A., Gorelenkov N.N. and White R.B. 2001 *Phys. Rev. Lett.* **87** 205003